NASA TECHNICAL NOTE

NASA TN D-3782

NASA TN D-3782

THREE-DIMENSIONAL PLASMA ACCELERATION THROUGH AXISYMMETRIC DIVERGING MAGNETIC FIELDS BASED ON DIPOLE MOMENT APPROXIMATION

by H. G. Kosmahl

Lewis Research Center

Cleveland, Ohio

NATIONAL AERONAUTICS AND SPACE ADMINISTRATION • WASHINGTON, D. C. • JANUARY 1967

NASA TN D-3782

THREE-DIMENSIONAL PLASMA ACCELERATION THROUGH AXISYMMETRIC DIVERGING MAGNETIC FIELDS BASED ON DIPOLE MOMENT APPROXIMATION

By H. G. Kosmahl

Lewis Research Center
Cleveland, Ohio

NATIONAL AERONAUTICS AND SPACE ADMINISTRATION

For sale by the Clearinghouse for Federal Scientific and Technical Information
Springfield, Virginia 22151 – Price $2.00

THREE-DIMENSIONAL PLASMA ACCELERATION THROUGH AXISYMMETRIC DIVERGING MAGNETIC FIELDS BASED ON DIPOLE MOMENT APPROXIMATION*

by H. G. Kosmahl

Lewis Research Center

SUMMARY

The acceleration of a tenuous plasma whose initial energy is stored in the magnetic dipole moments of the electrons immersed in a diverging magnetic field was investigated theoretically. Adiabatic conservation of the dipole moments and axisymmetric steady-state fields were assumed, and three-dimensional trajectories of the plasma and the induced space-charge fields were computed. The computations were carried out for atomic weights of 40 and 130. The particle trajectories cross the field lines, and the plasma emerges as a well-defined beam. From the amount of divergence in the beam, a propulsive efficiency is defined. This efficiency is primarily a function of the radius and the length of the solenoid and the position beyond the center of the magnetic field at which the plasma of a given radial extension is initially injected. Conditions for a favorable design of a propulsion device are shown, and the mechanism of the acceleration process is explained. Results agree well with experiments performed on a microwave-powered plasma accelerator working under conditions that approximate the theoretical assumptions. A significant conclusion of these studies is that trajectories are independent of the ionic mass and the magnitude of the dipole moment, that is, of the energy of the particles.

INTRODUCTION

The subject of this analytical study is a three-dimensional computation of electron-ion trajectories in a tenuous collisionless plasma. These computations are closely re-

---

*The material in this report is also published in J. Appl. Phys., no.

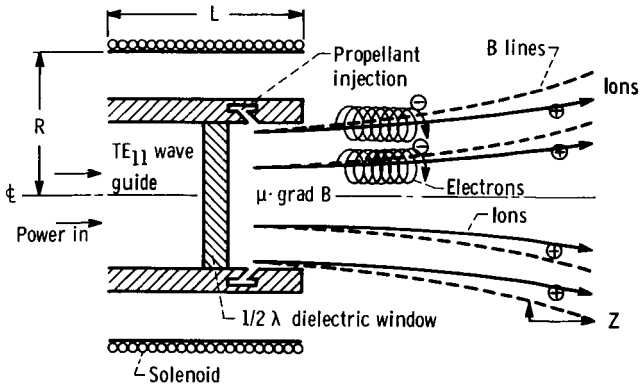

Figure 1. - Schematic diagram of accelerator.

lated to conditions existing in the experimental, microwave-powered accelerator described in reference 1. In the computations, a number of electrons, together with an equal number of ions, are injected with a constant velocity u_o along the field lines of a cylindrical solenoid (fig. 1). At the plane of injection, the B field is still closely parallel to the axis of symmetry. In the model, all injected electrons are assumed to possess an adiabatically invariant magnetic dipole moment μ parallel to B which is caused by the orbiting motion of the electrons around the B flux lines. Other important assumptions are that total initial plasma energy per particle is equal to $\frac{1}{2}\omega_c^2 r_c^2 \cdot m = \mu_o B_{res}$, δ-function distribution of the dipole moments around $\mu = \mu_o$, injection at a single plane $z = z_o$, single ionization of the species, absence of collisions, and zero initial angular momentum. (All symbols are defined in appendix A.)

For a given set of input conditions $\Re_o$ and $\dot{\Re}_o$, the trajectory of a charged particle in steady-state electromagnetic fields is described completely by the equation $m\ddot{\vec{\Re}} = \pm e(\vec{E} + \dot{\vec{\Re}} \times \vec{B})$ where $\Re$ and $\dot{\Re}$ are the radius vector and the absolute velocity of the particle itself, respectively. Because of the complex nature of the motion, composed of the superposition of the "spiraling" (corresponding to $\vec{\mu}$), the translating (r and $\dot{z}$), and the azimuthal (θ) components of the electron, it is easier to follow the method first suggested by Alfven (refs. 2 and 3): each particle is assigned a "substitute" trajectory described by the r, θ, and z motion of its guiding center while all the "spiraling" energy is considered as potential energy μB. Note that the θ motion of the guiding center must not be confused with the motion that produces μ.

As Hellwig has shown (ref. 4), μ is an adiabatic constant of motion at least to the second order in the derivatives of B in spatially and temporarily changing magnetic fields, if, taken over one cyclotron orbit, the change ΔB is small compared with B; that is, $\Delta B \ll B$. The validity of this assumption is examined in appendix C.

The actual motion of an electron is obviously more complicated than that of a substitute particle because of instabilities, oscillations, and random motion. Because space-charge neutrality must be preserved to a very high degree over regions equal to or larger than some few Debye shielding lengths λ_D, a substitute electron will be, on the average, in the vicinity of each ion. In a way, the ionic inertia mass M may be considered tied to the dipole moment μ of the substitute electron by way of space-charge forces.

Since any relative motion of electrons and ions in either the r or the z direction produces a charge separation, only the θ motion is unimpeded. Thus, the macroscopic ion and the substitute electron velocities and trajectories must remain substantially equal. Essentially, these conditions require a macroscopic space-charge neutrality and the disappearance of the current components $j_z = j_r = 0$, except j_θ, which does not equal zero. Since electrons can acquire, in general, any velocity $u < c$ with small energy expenditures, the expelling force on the magnetic dipole $(\vec{\mu} \cdot \vec{\nabla})\vec{B}$ must be closely opposed by the induced space charge-force $e\vec{E}$. This latter force serves, in turn, to expel (accelerate) the ions.

The ejection of a plasma out of magnetic fields has also been analyzed by Kilpatrick, et al. (ref. 5), who treated the plasma as a conducting continuum in thermal equilibrium. The result of Kilpatrick's studies is that the plasma follows the B lines and cannot free itself from the field unless a very small angle of divergence is maintained. The results of the present investigation show that, while the trajectories are strongly affected by the B field, even a collisionless plasma can free itself from the flux lines.

Although the problem of a three-dimensional acceleration of a plasma through axisymmetric diverging magnetic fields is presented in this study as a general model, numerical computations were carried out only for cases closely associated with the microwave-powered accelerator (ref. 1), which might be of practical importance to space propulsion; that is, $B_{res} \approx 3000$ gauss, $\omega_{c,res} \approx \omega_{rf} \approx 8.35$ gigahertz, $n(z_0) \approx 10^{12} - 5\times10^{12}$ particles per cubic centimeter, and $u_\infty \approx 5\times10^4$ meters per second, corresponding to a specific impulse of 5000 seconds.

TRAJECTORY EQUATIONS

Trajectory equations are obtained by solving simultaneously the momentum equations, the energy equations, the continuity equations, and the Poisson equation.

Momentum Equations

The momentum equations will be derived from a Lagrangian formulation of the problem. Cylindrical coordinates and azimuthal symmetry are assumed throughout. The generalized Lagrangian L^* of the guiding center can be written for electrons and ions, respectively, in the form

$$L_e^* = \frac{1}{2} m u_e^2 - e\left(\varphi_e - \vec{u}_e \cdot \vec{A}\right) \tag{1}$$

$$L_i^* = \frac{1}{2} M u_i^2 + e\left(\varphi_i - \vec{u}_i \cdot \vec{A}\right) \tag{2}$$

with the notations

$$\vec{u} = \hat{a}_r \dot{r} + \hat{a}_\theta r\dot{\theta} + \hat{a}_z \dot{z} \tag{3}$$

$$\varphi_e = -V + \frac{\vec{\mu} \cdot \vec{B}}{e} \tag{4a}$$

$$\varphi_i = -V \tag{4b}$$

For the electrodeless, steady-state model to be investigated, the following conditions are applied:

$$j_r = j_z = 0; \quad E_\theta = -\text{grad}_\theta V = 0; \quad \frac{\partial}{\partial t} = 0 \tag{5}$$

$$\vec{A} \equiv \hat{a}_\theta A; \quad \vec{B} = \text{curl } \vec{A} = \hat{a}_r B_r + \hat{a}_z B_z \tag{6}$$

In equation (6), any magnetic fields induced by the dipoles have been neglected as small compared with the external field produced by $\vec{A}$.

The momentum equations are obtained from

$$\frac{d}{dt}\left(\nabla_{\dot{q}} L^*\right) - \nabla_q L^* = 0 \tag{7}$$

where q and $\dot{q}$ are the coordinates and the rate of charge of coordinates, respectively, and $\nabla_{\dot{q}}$ and ∇_q are the corresponding gradient operators. From the assumption that μ is adiabatically invariant and $\frac{\partial}{\partial t} = \frac{\partial}{\partial \theta} = 0$ equations (7) and (1) yield the momentum equation for electrons:

$$\dot{\vec{u}}_e = \frac{e}{m}\left[-\nabla_q \varphi + u_e \times (\nabla \times \vec{A})\right] = \frac{e}{m}\left[+\nabla_q V - \left(\frac{\vec{\mu} \cdot \nabla_q}{e}\right)\vec{B} + \vec{u}_e \times \vec{B}\right] \tag{8}$$

Because of the assumption of the adiabatic invariance of μ, all the derivatives of μ are considered small compared with the derivatives of B and, consequently, are neglected in equation (8) and the following equations. From equations (7) and (2), the momentum equation for the ions is

$$\vec{u}_i = \frac{e}{M}\left[-\nabla_q V + u_i \times (\nabla \times \vec{A})\right] = \frac{e}{M}\left(-\nabla_q V + \vec{u}_i \times \vec{B}\right) \tag{9}$$

The term $\left(\frac{\vec{\mu} \cdot \nabla}{e}\right)\vec{B}$ represents a force, which shall be denoted as F. The components of F are

$$\left.\begin{aligned} F_r &= \mu_r \frac{\partial B_r}{\partial r} + 0 + \mu_z \frac{\partial B_r}{\partial z} \\ F_\theta &= 0 + 0 + 0 \\ F_z &= \mu_r \frac{\partial B_z}{\partial r} + 0 + \mu_z \frac{\partial B_z}{\partial z} \end{aligned}\right\} \tag{10}$$

with

$$\left.\begin{aligned} \vec{\mu} &= -\mu_o \frac{\vec{B}(r, z)}{|B(r, z)|} \\ \mu_o &= \text{constant} > 0 \end{aligned}\right\} \tag{11}$$

The induced dipole moment μ_o is antiparallel to the magnetic field and is thus negative.

With the help of equation (10), the r, θ, and z components of equations (8) and (9) become, for the electrons,

$$\ddot{r} = r\dot{\theta}_e^2 - \frac{e}{m}(E_r + B_z r\dot{\theta}_e) + \frac{F_{\mu r}}{m} \tag{12a}$$

$$\frac{1}{r}\frac{d}{dt}\left(r^2\dot{\theta}_e\right) = -\frac{e}{m}(B_r\dot{z} - B_z\dot{r}) \tag{12b}$$

$$\ddot{z} = -\frac{e}{m}(E_z - B_r r\dot{\theta}_e) + \frac{F_{\mu z}}{m} \tag{12c}$$

and for the ions,

$$\ddot{r} = r\dot{\theta}_i^2 + \frac{e}{M}(E_r + B_z r\dot{\theta}_i) \tag{13a}$$

$$\frac{1}{r}\frac{d}{dt}\left(r^2\dot{\theta}_i\right) = +\frac{e}{M}(B_z\dot{z} - B_z\dot{r}) \tag{13b}$$

$$\ddot{z} = +\frac{e}{M}(E_z - B_r r\dot{\theta}_i) \tag{13c}$$

Next, in integrating equations (12b) and (13b) use is made of Busch's theorem in axisymmetric fields (ref. 6). For electrons and ions, respectively, one obtains:

$$m(r^2\dot{\theta})_e = +e\left[\psi(r, z) - \psi_o(r_o, z_o)\right] \tag{14a}$$

and

$$M(r^2\dot{\theta})_i = -e\left[\psi(r, z) - \psi_o(r_o, z_o)\right] \tag{14b}$$

where

$$\psi(r, z) \equiv \int_0^r B_z(r, z) r\, dr \tag{15a}$$

$$\psi_o(r_o, z_o) = \int_0^{r_o} B(r, z_o) \cdot r\, dr \tag{15b}$$

The initial angular momentum $mr_o^2\dot{\theta}_o$ or $Mr_o^2\dot{\theta}_o$ of the guiding centers in equations (14) has been set equal to zero, in accordance with the assumption that the dipoles and the ions are injected with zero angular velocity. Equations (14) are used to eliminate $\dot{\theta}$ from equations (12) and (13) in the computations.

Energy Equations

The energy equations are obtained by multiplying equations (8) and (9) by u_e or u_i, respectively:

$$\frac{1}{2}\frac{d}{dt}(u_e)^2 = +\frac{e}{m}\frac{dV}{dt} - \frac{1}{m}\vec{\mu}\frac{d\vec{B}}{dt} = \frac{e}{m}\frac{d}{dt}\left(V - \frac{\vec{\mu}\cdot\vec{B}}{e}\right) = -\frac{e}{m}\frac{d\varphi_e}{dt} \tag{16}$$

$$\frac{1}{2}\frac{d}{dt}(u_i)^2 = -\frac{e}{M}\frac{dV}{dt} = \frac{e}{M}\frac{d\varphi_i}{dt} \tag{17}$$

Equations (16) and (17) are easily integrated to

$$\frac{m}{2}\left[u_e^2(r, z, \theta_o) - u_o^2\right] = \vec{\mu}\cdot\left[\vec{B}_o(r_o, z_o) - \vec{B}(r, z)\right] - e\left[V(r, z) - V_\infty(r, z)\right] \tag{18}$$

and

$$\frac{M}{2}\left[u_i^2(r, z, \theta_o) - u_o^2\right] = e\left[V(r_o, z_o) - V_\infty(r, z)\right] \tag{19}$$

For $z \to \infty$, B_∞ and grad B_∞ as well as grad V approach zero. The plasma is assumed to have a reference potential $V_\infty = 0$ at $z \to \infty$.

Continuity Equation

The continuity equation is developed with the help of figure 2. As a consequence of zero net current, $j_z = j_r = 0$ and macroscopic space-charge neutrality $\rho_{net} \approx 0$, $u_e(r, z)$ must be always close to or identical with $u_i(r, z)$. Thus, $u(r, z) \approx u_e(r, z) \approx u_i(r, z)$. In figure 2 a current density $\pm\rho_o u_o$ (the signs indicating ions or electrons, respectively) is injected perpendicular to the plane $z = z_o$ between r_o and $r_o + dr$. The current dI_o through this annular ring of area $2\pi r_o\, dr_o$ is

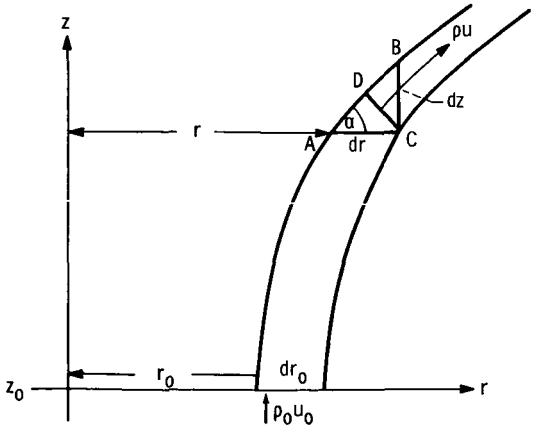

Figure 2. - Derivation of continuity equation.

$$dI_o = \pm 2\pi\rho_o u_o r_o\, dr_o \tag{20}$$

To calculate dI, the current between r and r + dr perpendicular to DC, it must be noted from figure 2 that

$$\tan\alpha = \frac{1}{r'},\quad DC = dr\cdot\sin\alpha = \frac{dr}{\sqrt{1 + (r')^2}}$$

where

$$r' = \frac{dr}{dz}$$

The current through the ring between r and r + dr perpendicular to DC is, therefore,

$$dI = \pm\rho(r, z) \cdot u(r, z) \cdot 2\pi r\, dr \cdot \sin\alpha = \pm 2\pi r\, dr \rho u(r, z) \frac{1}{\sqrt{1 + (r')^2}} \tag{21}$$

Note that motion in the θ direction does not enter the charge conservation in the continuity equation. Thus, $u(r, z) = \left(\dot{r}^2 + \dot{z}^2\right)^{1/2}$ must be used in equation (21). When equations (20) and (21) are set equal, the expression for $\pm\rho(r, z)$ is

$$\rho(r, z) = \pm \frac{\rho_o u_o \cdot r_o \frac{dr}{dr_o} \sqrt{1 + (r')^2}}{r \cdot u(r, z)} \tag{22}$$

dr/dr_o and r' may be obtained from the trajectories and u from equation (18) or (19).

Poisson Equation

Induced space-charge potential V is calculated from the Poisson equation:

$$\frac{\partial^2 V}{\partial r^2} + \frac{1}{r}\frac{\partial V}{\partial r} + \frac{\partial^2 V}{\partial z^2} = -\frac{\rho_e + \rho_i}{\epsilon_o} \tag{23}$$

The boundary conditions neglect any surface charges since an entirely electrodeless system in a free space is assumed.

CALCULATION OF BEAM DIVERGENCE EFFICIENCY

If particle trajectories are assumed known throughout the entire exhaust region including infinity, a "divergence" efficiency η_D, which is defined as the ratio of the directed kinetic energy of the stream at infinity to the total kinetic energy, can be calculated from

$$\eta_D = \frac{1}{\dot{N}} \sum_{1}^{\dot{N}} \frac{\dot{z}^2}{\dot{z}^2 + \dot{r}^2} f_w = \frac{1}{\dot{N}} \sum_{1}^{\dot{N}} \frac{f_w}{1 + (r')^2} \tag{24}$$

where $\dot{N}$ represents the number of particles injected per second. That there is no azimuthal energy $Mr^2\dot{\theta}_i$ at infinity should be noted.

The function f_w introduced in equation (24) is a weighting function representing the number density of particles injected initially between r_o and $r_o + dr_o$ per unit time such that

$$\frac{2\pi}{\dot{N}} \int_0^{D/2} f_w r_o \, dr_o = 1 \tag{25}$$

Two cases are examined here. First, if the propellant injection density n_o at $z = z_o$ were constant across the waveguide, there would be $2\pi n_o u_o r_o \, dr_o$ particles injected per second between r_o and $r_o + dr_o$. Thus, $f_w = n_o u_o$.

Since $r'(r_o)$ is known along the trajectory and is continuous across the injection plane, the summation in equation (24) may be replaced by an integral and the following is obtained for η:

$$\eta_{D26} = \frac{\frac{2\pi}{\dot{N}} n_o u_o \int_{r_o=0}^{r_o=1.4} \frac{r_o \, dr_o}{1 + \left[r'(r_o)\right]^2}}{\frac{2\pi}{\dot{N}} n_o u_o \int_{r_o=0}^{r_o=1.4} r_o \, dr_o} \tag{26}$$

The second case assumes that the propellant is injected preferentially along the axis $r \approx 0$ in such a manner that $n_o = \frac{\alpha}{r_o}$, where α is a proportionality constant. The efficiency becomes

$$\eta_{D27} = \frac{\frac{2\pi}{\dot{N}} \alpha \int_{r_o=0}^{r_o=1.4} \frac{dr_o}{1 + \left[r'(r_o)\right]^2}}{\frac{2\pi}{\dot{N}} \alpha \int_{r_o=0}^{r_o=1.4} dr_o} \tag{27}$$

The actual propellant injection density in the quoted experiments lies somewhere between the two cases.

SOLUTION OF EQUATIONS

The preceding equations (12), (13), (14), (15), (18), (19), (22), and (23), constitute in a mathematical sense a complete and uniquely defined set of expressions for a given external magnetic field. Although this set of equations is solvable in principle, the general behavior and the order of magnitude of the solutions must be determined a priori in order to make the computational program tractable. This problem is dealt with in detail in appendix B.

The range of parameters and numerical values chosen for the computations corresponds to that for the accelerator of reference 1. The driving microwave frequency f is 8.35 gigahertz. Consequently, a peak magnetic field $B > 3100$ gauss is necessary for achieving the resonance condition $\omega_{rf} \approx \omega_c$. Peak values of B were chosen in these computations to permit the resonance to occur at $z_0 = 2.5$ and $z_0 = 5.0$ centimeters.

The static magnetic field B was calculated from the expression for the vector potential $\vec{A}$ of a single layer solenoid of radius R and length L wound only in the θ direction. The equation for A_θ is (ref. 7)

$$A_\theta = C \int_0^\infty I_1(kR)K_1(kr)\cos kz \sin \frac{kL}{2} \frac{dk}{k} \qquad \text{for } r > R \tag{28a}$$

and

$$A_\theta = C \int_0^\infty K_1(kR)I_1(kr)\cos kz \sin \frac{kL}{2} \frac{dk}{k} \qquad \text{for } r < R \tag{28b}$$

Thus,

$$B(r, z) = \nabla \times A_\theta$$

The constant C is determined from the condition that at the origin

$$r = z = 0, \quad B(0, 0) = B_0$$

Most experiments were carried out with argon and xenon, with mass flow rates between 0.5 and 2.0 milligrams per second and power levels between 500 and 2000 watts. From these numbers and the atomic masses $M_{argon} = 6.68\times10^{-26}$ kilogram and $M_{xenon} = 21.95\times10^{-26}$ kilogram the injection rate in particles per second $\dot{N}$ lies between 10^{18} and 10^{19} atoms per second and an energy per particle $P/\dot{N}$ lies between 5×10^{-17} and 2×10^{-15} joule.

The value μ_o can then be calculated from $\mu_o \approx \frac{P/\dot{N}}{B_{res}}$ by assuming a δ function distribution of μ and no energy losses. The variation of μ_o is between 2×10^{-12} and 60×10^{-12} ampere - square centimeter. Because of the accent on low specific impulse, the range selected for computations was approximately 2×10^{-12} to 8×10^{-12} ampere - square centimeter.

The plasma "diameter" at the injection plane is identical with the diameter D of the circular waveguide in the TE_{11} mode for an X-band frequency range; that is, D = 2.8 centimeters. If it is assumed temporarily that the injected plasma fills the waveguide cross section evenly and that it is injected with a sonic velocity u_o at room temperature. The propellant density n_o can be obtained from $n_o \approx 4\dot{N}/(\pi D^2 \cdot u_o)$ and amounts to a few times 10^{12} per cubic centimeter for $u_o = 1.7\times10^2$ to 3×10^2 meters per second. The limit for $n_o(\omega_p \leqq \omega_{rf})$ is approximately $n_o \approx 5\times10^{12}$.

The computational step in computing the trajectories was 0.1 centimeter for r and 0.5 centimeter for z.

The entire computational loop used in solving the equations consisted of the following major steps:

(1) B-field, equations (28a), (28b), and (6), and the dipole force field F (eq. (10)) were mapped.

(2) Flux integrals (15a) and (15b) were computed.

(3) First approximations to trajectories from the condition ψ = constant were found.

(4) Laplace and Poisson equation (23) were solved on axis.

(5) The potential V was mapped off axis.

(6) A more accurate trajectory was computed.

(7) A more accurate V-field was computed.

DISCUSSION OF RESULTS

The results of the computations are presented in figures 3 to 5. Figure 3(a) shows the trajectories for argon and xenon injected at $z_o = 2.5$ centimeters, and figure 3(b) shows the same trajectories for an injection at $z_o = 5.0$ centimeters. Figure 4 shows fields and potentials for various values of μ_o. All figures were computed for a

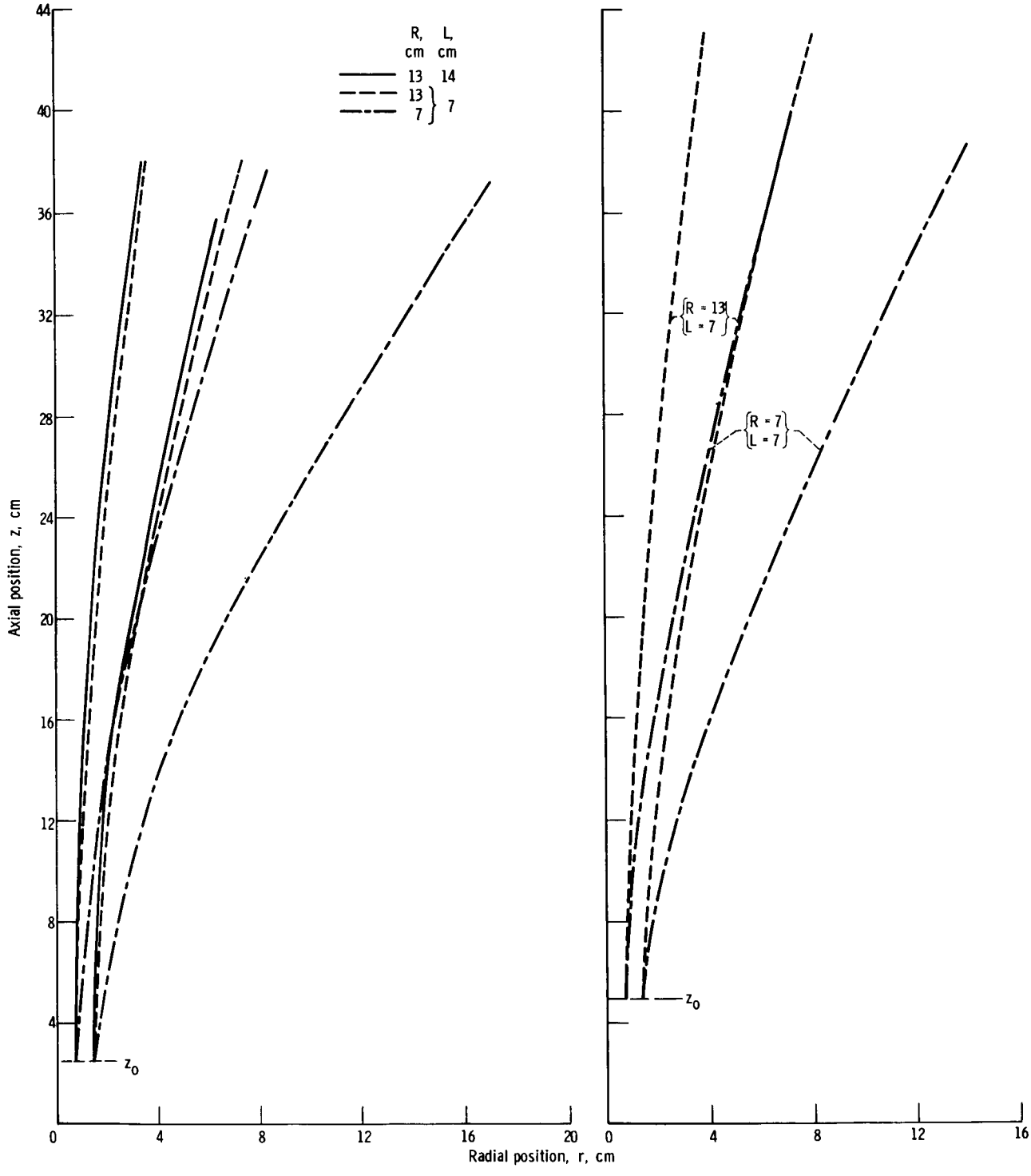

(a) z_0 = 2.5 centimeters.

(b) z_0 = 5.0 centimeters.

Figure 3. - Trajectories of seventh (r_0 = 0.7 cm) and fourteenth (r_0 = 1.4 cm) argon and xenon particles for three solenoid geometries.

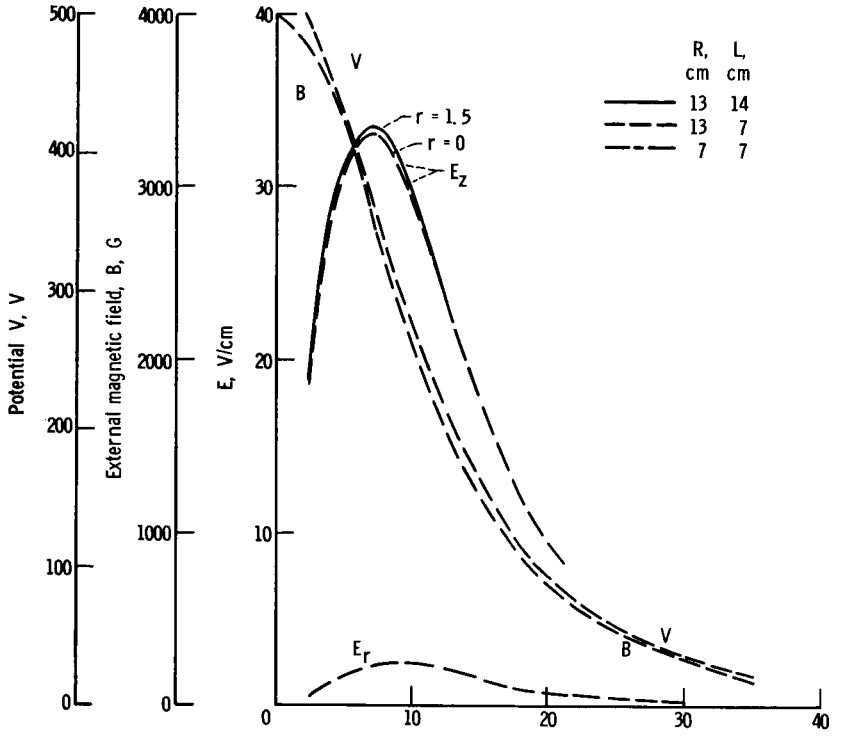

(a) $\mu_0 = 2.08 \times 10^{-12}$ ampere-square centimeter; $z_0 = 2.5$ centimeters. E_z on axis and E_z at r = 1.5 centimeters.

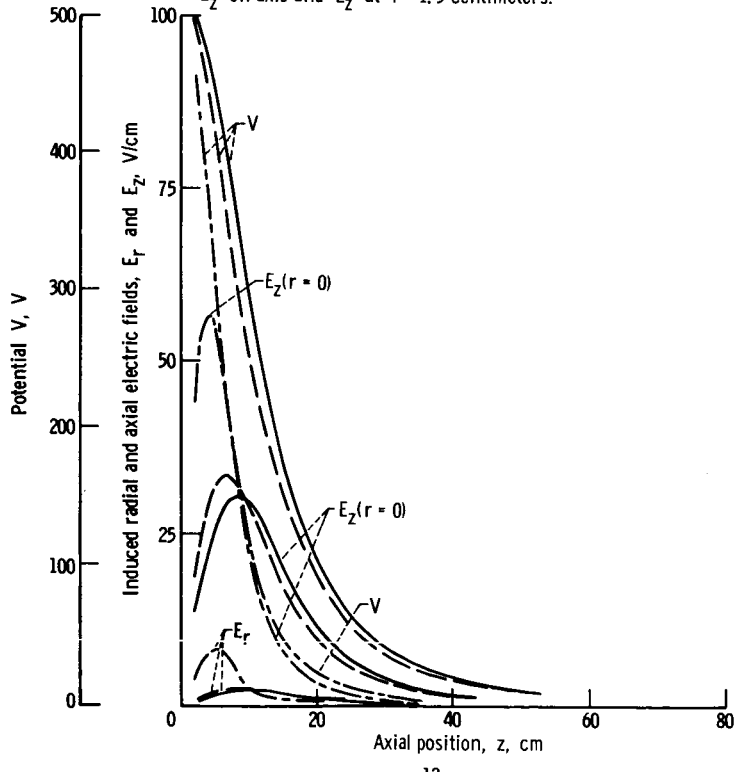

(b) V on axis; $\mu_0 = 2.08 \times 10^{-12}$ ampere-square centimeter; z_0 = 2.5 centimeters.

Figure 4. - Magnetic field B, induced voltage V, induced radial electric field E_r, and induced axial electric field E_z against distance z for three solenoid geometries. E_r at r = 1.5 centimeters.

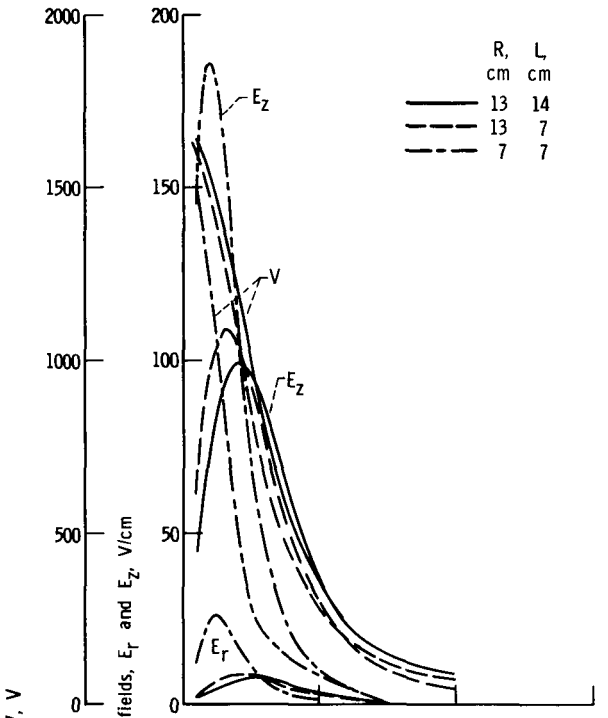

(c) V and E_z on axis; $\mu_0 = 6.85 \times 10^{-12}$ ampere-square centimeter; $z_0 = 2.5$ centimeters.

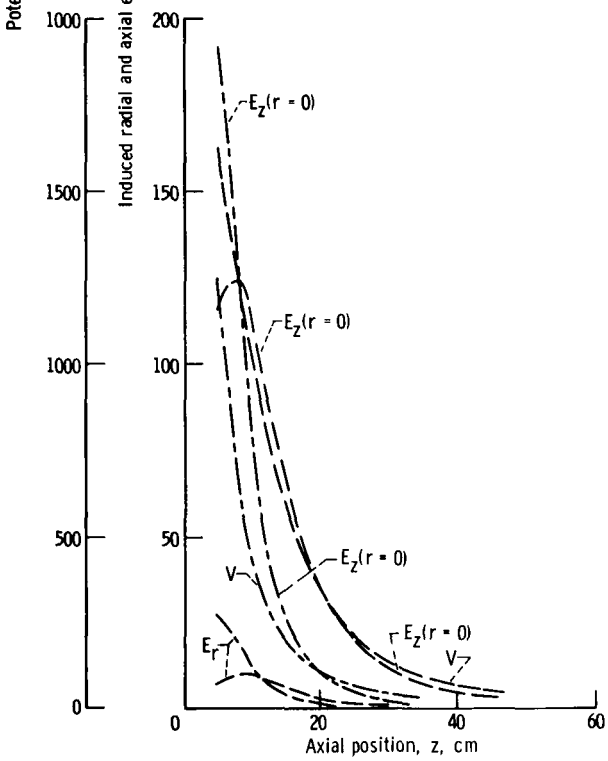

(d) $\mu_0 = 7.82 \times 10^{-12}$ ampere-square centimeter; $z_0 = 5$ centimeters.

Figure 4. - Concluded.

magnetic field of peak value $B_0 \approx 4000$ gauss, but for three different dimensions of the field producing solenoid: R = 7, L = 7; R = 13, L = 14; and R = 13, L = 7 centimeters.

The following conclusions can be deduced from a review of the results:

(1) For equal R, L, and z_0 and the same initial plasma injection radius, the macroscopic trajectories are independent of the ionic mass M and the magnitude of the dipole moment μ_0 (fig. 3). The range of μ was approximately 2×10^{-12} to approximately 8×10^{-12} ampere - square centimeter.

(2) The trajectories depend on R, L, and z_0, and their slope r' is increasing with decreasing R and L for a fixed plasma injection diameter. Comparing figure 3(a) with figure 3(b) shows, in addition, that the slope r' also increases with decreasing z_0.

(3) The induced voltage V is always near-proportional to the magnetic induction B (fig. 4).

(4) The induced electric field E_z is almost independent of the radial position r (fig. 4) and peaks in the neighborhood of $z \approx L/2$ (figs. 3(a) to (c)). The maximum of E_z and of E_r vary with the gradient of B and, thus, vary inversely with the solenoid dimensions R and L.

(5) For a fixed magnet geometry and field the induced potentials and electric fields are independent of the ionic mass M and proportional to μ, which in turn is determined only by the ratio $P/\dot{N}$, in accord with the assumptions of a monoenergetic plasma. The difference in the calcu-

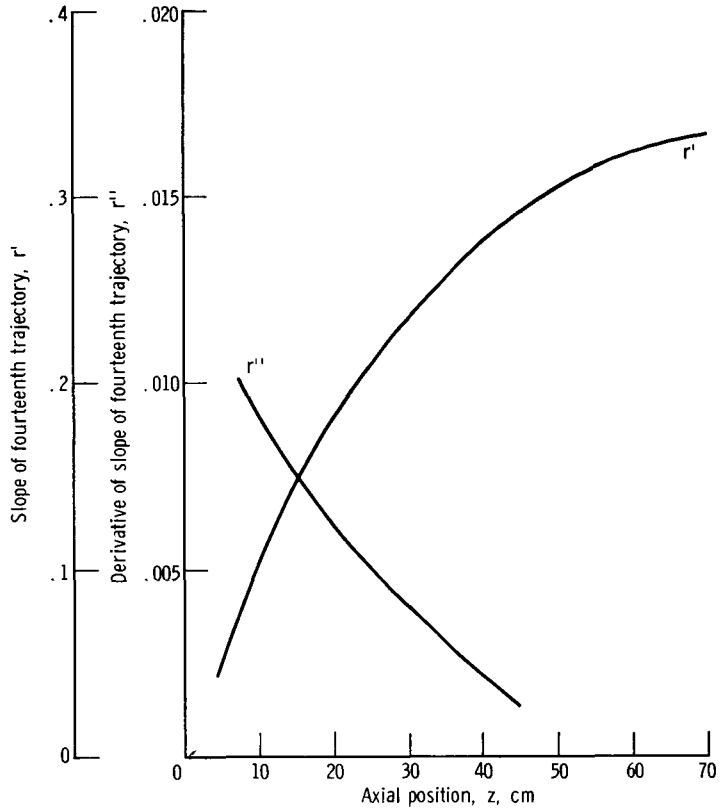

Figure 5. - Slope r' and derivative of slope r'' of fourteenth particle (r_0 = 1.4 cm) against distance z for solenoid R = 13 centimeters, L = 7 centimeters; z_0 = 2.5 centimeters.

lated potentials for the same μ results from local differences in the value of B in the injection plane and from a different location of z_0 of the plane itself (figs. 3(b) to (d)).

(6) The plasma exhaust velocity is approximately equal to $u_\infty \approx \sqrt{2\mu_0 B_{res}/M}$ and depends only on the ratio μ/M, but not, however, on μ and M individually, as long as $M >> m$.

(7) Figure 5 is a plot of r' and r'' for the outermost particle as a function of z for one selected case demonstrating the convergence of the trajectory solutions. As r' converges asymptomatically to its final value, r'' approaches zero. In figures 3(a) and (b), the trajectories are approaching straight lines at axial distances $z \gtrsim 20$ to 40 centimeters.

(8) The discontinuity in E in figures 4(a) to (c) at $z = z_c$ results from the discontinuous introduction of the magnetic dipoles and is equivalent to a sudden space-charge force acting at z_0. In a real accelerator, such a discontinuity is "smoothed" out and E is continuous.

(9) The azimuthal velocity of the ions $r\dot{\theta}_i$ is less than 3 centimeters per second everywhere, and that of the electrons $r\dot{\theta}_e = \frac{M}{m} r\theta_i$ is on the order of 10^5 to 10^6 centi-

TABLE I. - EFFICIENCIES

Initial axial injection position, z_o, cm	Ratio of radius to length, R/L, cm	Efficiency, η	
		Equation (27)	Equation (28)
2.5	13/14	0.974	0.964
	13/7	.971	.960
	7/7	.920	.880
5.0	13/14	-----	-----
	13/7	0.975	0.964
	7/7	.943	.90

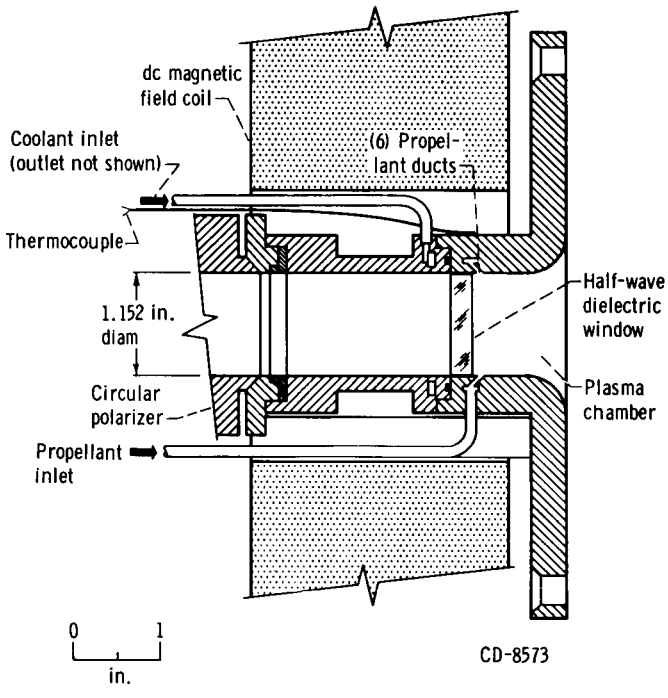

Figure 6. - Electron cyclotron resonance accelerator; 8.35 gigahertz.

meters per second. Both velocities approach zero at large values of z in accordance with equation (14).

(10) The efficiencies, as defined in equations (27) and (28), are tabulated in table I for $z_o = 2.5$ and 5.0 centimeters, three R, L values for the solenoid, and a waveguide diameter D = 2.8 centimeters. The loss of directed beam energy resulting from the divergence of the plasma exhaust is not critical as long as $2R/D \geq 5$. A noticeable effect of z_o on η also occurs. The improvement of η with increasing z_o is the result of much less entrapped initial flux for a given solenoid, so that less divergence occurs.

COMPARISON WITH EXPERIMENTAL DATA

The available experimental data which were obtained with the accelerator pictured in figure 6 permit the following comparisons with theory: divergence angle of the exhaust and its independence of the ionic mass M, slope of the induced space-charge potential V, and the magnitude of V.

Figure 7 shows typical photographs of the visible plasma exhaust produced on a photographic plate by argon and krypton propellants. The solenoid geometry was R = 13 centimeters and L = 7 centimeters. (While the luminous beam edge itself is very clear, its photograph is not because of fluctuations during the exposure time.) Of particular interest is the divergence angle of the outermost trajectory (r_o = 1.4 cm, beam edge), which is drawn in figure 7 as the angle γ. In good agreement with the exit angle γ in figure 3, which is approximately 18^o, r_o = 1.4 centimeters, R = 13 centimeters, L = 7 centimeters, γ is found to be approximately 19^o to

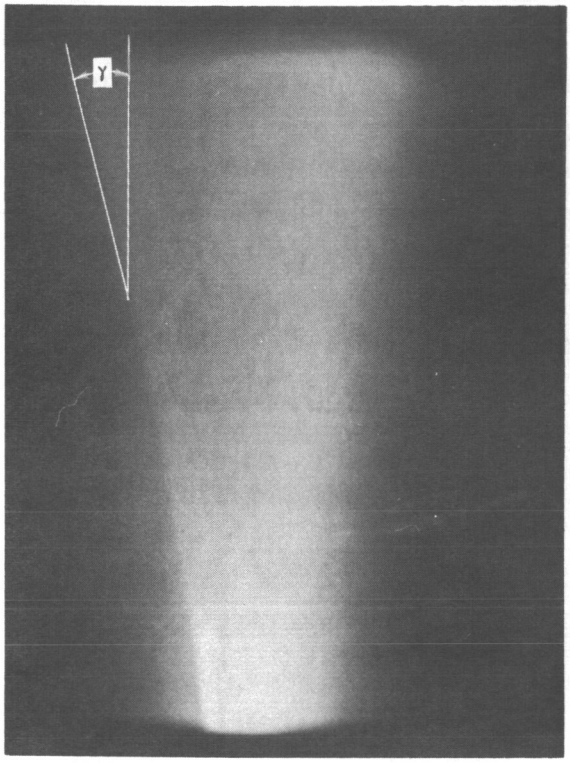

(a) Argon. Gas flow rate, 0.93 milligram per second.

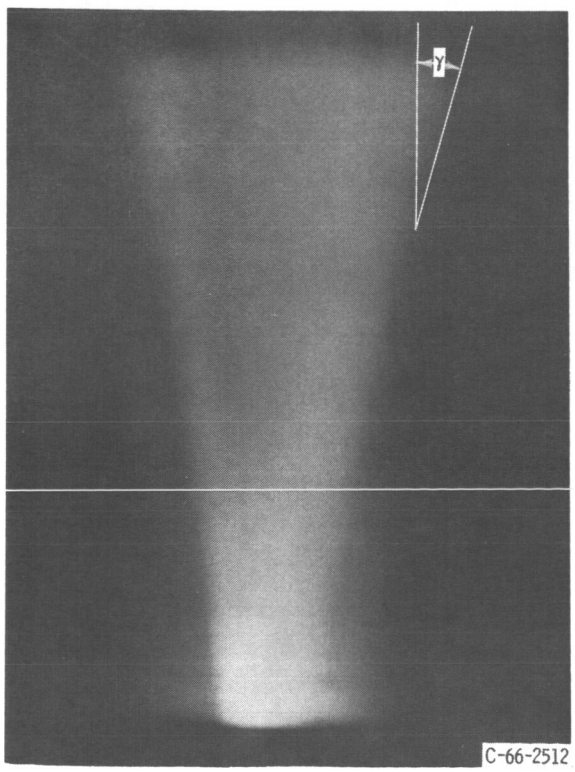

(b) Krypton. Gas flow rate, 1.48 milligrams per second.

Figure 7. - Exhaust stream. Coil current, 210 amperes; power, 1 kilowatt radio frequency.

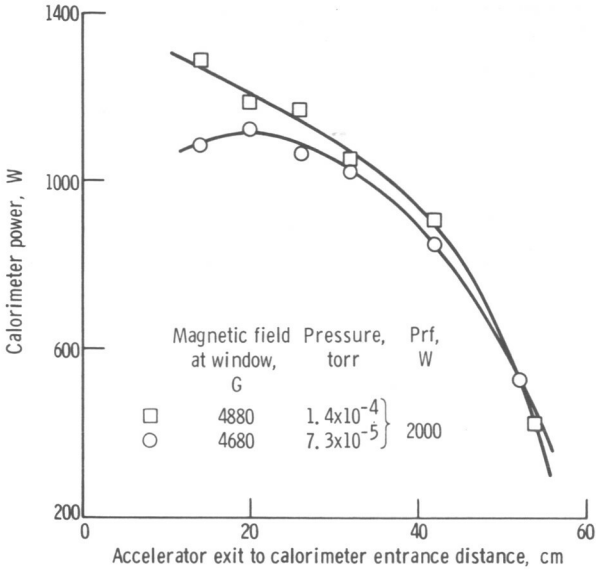

Figure 8. - Dependence of calorimeter power on calorimeter position. Propellant, xenon; calorimeter, 10 inch diameter by 20 inch length.

Curve	Mass flow, mg/sec	Accelerator exit to array distance, cm
1	1.07	72
2	.87	112
3	.76	152
4	.97	192

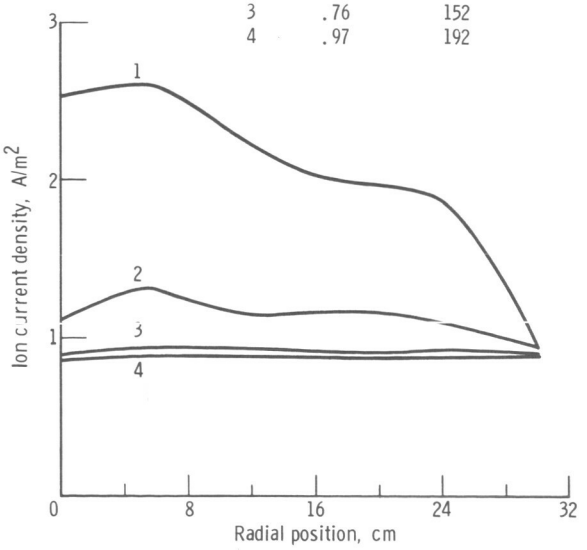

Figure 9. - Exhaust stream ion current density profiles at several axial positions as determined by diode tube array. Propellant, argon; radiofrequency power, 684 watts.

20° in figure 7 and is quite independent of the ionic mass. Additional evidence (ref. 1) from calorimetric sampling of the exhaust (fig. 8) and ion density measurements (fig. 9) shows that the luminous beam is near-representative of the actual exhaust stream.

From figure 4, it was theoretically concluded that V is proportional to B. Figures 10(a) and (b) are experimental plots of the axial magnetic field and the induced plasma potential for argon and xenon, respectively. Over the measured region, V is near-proportional to B. In figure 10(b), the measured potential flattens out at $z > 25$ centimeters instead of following B. This deviation, however, is the result of an excessive

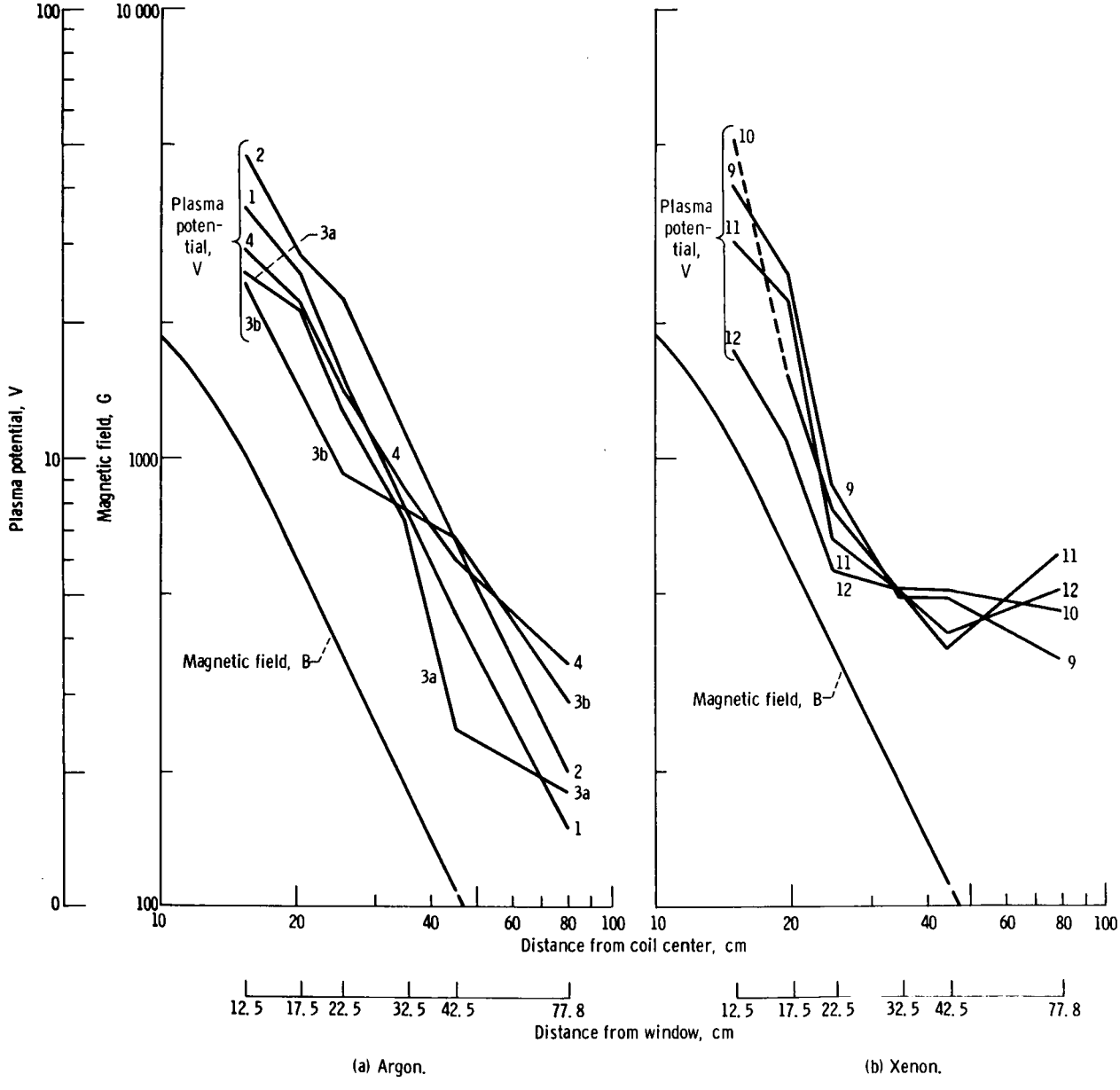

Figure 10. - Magnetic field and plasma potential profiles against distance. Radiofrequency power, 1 kilowatt. (Numbers from operating conditions listed in Table VII, ref. 1).

background pressure (ref. 1) due to diffusion and charge-exchange processes which tend to short out V.

The magnitude of the induced space-charge potentials should, according to figures 4(a) to (c), range from approximately 150 to approximately 500 volts at axial positions between z = 15 centimeters and z = 40 to 50 centimeters. From figures 10(a) and (b), on the other hand, only a potential drop of about 50 volts can be deduced. This large disagreement is not yet fully understood. Processes that could affect the calculations include background pressure effects, diffusion processes, ionization and excitations, instabilities, oscillations, a distribution in μ_0, and all direct energy losses. Furthermore, the driving microwave is known to be imperfectly polarized and its E field is not constant across the waveguide. Also, other modes than the "desirable" TE_{11} must appear in the vicinity of the waveguide edge, where a transition from a bounded TE_{11} wave into a free space wave occurs. Finally, ionization and energizing of the dipoles do not occur suddenly at a single injection plane z_0, but rather take place over a finite distance on the order of a few centimeters.

CONCLUSIONS

The following conclusions can be drawn from the results of a study of three-dimensional plasma acceleration through axisymmetric diverging magnetic fields:

1. The particle trajectories do cross the flux line, and come out in a well-defined, slightly diverging beam.

2. The trajectories depend on solenoid geometry and position of injection, and their slope increases with increasing plasma cross section relative to solenoid dimensions.

3. To keep thrust losses resulting from beam divergence small, the plasma diameter should not exceed one-fifth of the solenoid diameter, and the injection plane should be moved out axially toward the magnet face.

4. For the same solenoid geometry, the same plane of injection relative to the center of the magnetic field, and the same plasma diameter, the trajectories do not depend on the ionic mass and the dipole moment of the plasma electrons. The induced electric fields are a function of the electron injection energy only.

5. The induced space-charge potential is proportional to the product of the magnetic field times the dipole moment and is only weakly dependent on the radial position.

6. To obtain physically sensible solutions, the initial enclosed flux must be larger than the flux at an exit plane.

Lewis Research Center,
National Aeronautics and Space Administration,
Cleveland, Ohio, July 13, 1966,
120-26-03-00-22.

APPENDIX A

SYMBOLS

$\vec{A}$	magnetic vector potential
$\hat{a}_r, \hat{a}_z, \hat{a}_\theta$	unity vectors
$\vec{B}$	curl $\vec{A}$, magnetic field/ $T = 10^8$ G
B_{res}	magnetic field for electron cyclotron resonance
C	computation constant
c	speed of light, 3×10^8 m/sec
D	defined in fig. 2
$\vec{E}$	gradient of V, electric field, V/cm
e	1.6×10^{-19} coulomb
F	magnetic force on dipole, N
f_w	weighting function
I	current, A
$I_1(k_r)$	modified Bessel function of first kind and first order
j	current density, A/cm^2
$K_1(k_r)$	modified Bessel function of second kind and first order
k	Fourier wave number
L	length of solenoid, cm
L^*	generalized Lagrangian
M	mass of ion
m	rest mass of electron, 9.11×10^{-28} g
$\dot{N}$	ion (atom) injection rate, particles/sec
n	particle density, cm^{-3}
P	power
P_r	power radiated in cyclotron radiation
q, $\dot{q}$	coordinates, rate of change of coordinates
R	radius of solenoid, cm
$\mathcal{R}$	radius vector of particle
r_c	electron cyclotron radius
r, z, θ	cylindrical coordinates
$\vec{s}$	path element
t	time
u	$\hat{a}_r\dot{r} + \hat{a}_\theta r\dot{\theta} + \hat{a}_z\dot{z}$ - velocity, cm/sec
V	potential, V
v	transverse velocity of electron in cyclotron orbit
y	$r\dot{\theta}_e$ - azimuthal electron velocity
α	injection constant
δ	Dirac δ function
ϵ_o	8.86×10^{-14} F/cm
η_D	divergence efficiency
$\vec{\mu}$	magnetic dipole moment, (A) (cm^2)
ρ	space-charge density, $coulomb/cm^3$
τ_c	$2\pi/\omega_c$

φ generalized potential, V

ψ $\int_0^r B_z(r, z)r\, dr$, magnetic flux/2π

ω frequency

ω_c cyclotron frequency, e/mB

ω_p plasma frequency, $5.6\times10^4\ n_e^{1/2}$

ω_{rf} radian frequency, cps

Subscripts:

e electron

eff effective

i ion

net neutrality

o initial

res resonant

r, z, θ cylindrical coordinates

∞ final

Superscripts:

$\cdot$ total time derivative, $\frac{\partial}{\partial t} + \vec{u} \cdot \frac{\partial}{\partial \vec{s}}$

$'$ partial spatial derivative, $\partial/\partial z$

$''$ second spatial derivative

APPENDIX B

APPROXIMATIONS FOR INITIATION OF COMPUTER PROGRAMS

In this section, a number of approximate expressions will be developed and order of magnitude estimates will be established for the initiation of a computational program on the IBM 7094, in order to make it tractable.

The character of the force F on the electrons (eq. (10)) should be considered first. In the vicinity of the axis $F_z \approx \mu_z \cdot \frac{\partial B_z}{\partial z}$ and is positive since both μ_z and $\frac{\partial B_z}{\partial z}$ are negative. The predominant term in F_r is $\mu_z \frac{\partial B_r}{\partial z}$, which is negative over the initial most important range of acceleration. As defined in the equations the electrically induced field E_z and E_r is considered positive if it accelerates the ions in the positive z and r direction. Subtracting equation (13a) from equation (12a) and neglecting corresponding terms divided by M as compared with those divided by n yields

$$\ddot{r}_e - \ddot{r}_i \approx r\dot{\theta}_e^2 - eE_r - B_z r\dot{\theta}_e + \frac{F_r}{m} \approx 0 \tag{B1}$$

because $\ddot{r} = r'' \cdot \dot{z}^2 + r'\ddot{z}$ must be almost identical for ions and substitute electrons so that the left side of equation (B1) is approximately zero. The symbol y will be substituted for $r\dot{\theta}_e$ and treated for the moment as the only unknown in equation (B1). The quadratic equation

$$y^2 - r\left(\frac{e}{m} B_z\right) \cdot y - r \frac{e}{m}\left(E_r - \frac{F_r}{e}\right) = 0 \tag{B2}$$

has two roots

$$y_{\pm} = \frac{r \frac{e}{m} B_z}{2}\left[1 \pm \sqrt{1 + \frac{4\left(E_r - \frac{F_r}{e}\right)}{r \frac{e}{m} B_z^2}}\right] \tag{B3}$$

For r on the order of a few centimeters the term $\frac{E_r - \frac{F_r}{e}}{r \frac{e}{m} B_z^2}$ is on the order of 10^{-6} be-

cause E_r and F_r/e are both less than 10 volts per centimeter. Thus, very accurately

$$r\dot{\theta}_{e+} = y_+ \approx r\left(\frac{e}{m} B_z\right) + \frac{E_r - \dfrac{F_r}{e}}{B_z} \tag{B4a}$$

$$r\dot{\theta}_{e-} = y_- \approx \frac{\dfrac{F_r}{e} - E_r}{B_z} \tag{B4b}$$

The first term in equation (B4a) is (for B on the order of kilogauss) substantially larger than the second term and the kinetic energy $\frac{1}{2} m\dot{y}_+^2$ can assume any arbitrarily large values, which are determined only by the amount of B. This situation cannot be true, in general, and equation (B4a) must therefore be rejected. Notice also that the total energy of the plasma in our model cannot exceed $\mu_0 B_{res}$ per particle. Equation (B4b), on the other hand, admits any arbitrarily small value for y and represents, therefore, the only acceptable solution.

As mentioned before, $F_r < 0$ in the region where B and therefore E are large, the last term in equation (B2) is therefore positive, and the first term y^2 is positive but small because of our choice of equation (A4b). The term $r\frac{e}{m} B_z y = \frac{e}{m} B_z r^2\dot{\theta}$ must therefore be negative, or $r^2\dot{\theta} < 0$, which is possible only if, in equation (14a),

$$\psi(r, z) < \psi_0(r_0, z_0) \tag{B5}$$

The inequality equation (A5) is of fundamental importance, for it shows that the plasma must follow a tube of a slightly decreasing flux in order to obtain physically compatible solutions. If $(F_r/e) - E_r$ is looked upon as being an effective electric field $E_{r,eff}$, then equation (B4b) may be regarded as the θ component of $\vec{E}_{eff} \times \vec{B}/B^2$ drift. At larger values of z, F_r is no longer negative; however, E_r remains positive and $|E_r| > \left|\frac{F_r}{e}\right|$, so that the last term in equation (B2) is less than 0 and the compatibility conclusion made earlier is still valid. Thus, the plasma trajectories do not strictly follow magnetic flux lines, and because they do not, the plasma can free itself from magnetic fields.

Addition of equation (14a) and (14b) leads to

$$mr^2\dot{\theta}_e + Mr^2\dot{\theta}_i = 0 \tag{B6}$$

which means that the total angular momentum of the plasma is zero if it was zero at the

injection plane. This latter assumption of zero initial angular momentum is very reasonable for the case considered here as well as for a number of other cases with realistic injection schemes.

Equation (B6) determines, because r_e very closely equals r_i, the angular momentum of the ion species after $r^2\dot{\theta}_e = ry$ has been calculated from equation (B4b). The calculations of E_z and E_r are discussed next. On the axis $E_r = B_r = 0$. Since the space-charge densities ρ_e and ρ_i in equation (23) must be equal to within 10^{-10} or less in order that the induced voltages be around a few kilovolts or less, the ion and electron velocities must almost be equal everywhere. Thus, from equaling equations (12c) and (13c) the following is obtained:

$$E_z = \frac{F_z}{e} = \frac{\mu_o}{e} \cdot \frac{B_z}{B} \frac{\partial B_z}{\partial z} = \frac{\mu_o}{e} \frac{\partial B_z}{\partial z} \tag{B7}$$

on the axis, and $E_z \approx F_z/e$ elsewhere as long as $B_r < B_z$. For the latter condition, $F_r \approx \mu_z \frac{\partial B_r}{\partial z} = \frac{B_z}{|B|} \frac{\partial B_r}{\partial z}$, and if a similar argument is applied to equations (12a) and (13a), the following may be written as a fair approximation, which is better than an order of magnitude:

$$\frac{E_r}{E_z} \approx \frac{F_r}{F_z} \approx \frac{B_r}{B_z} \tag{B8}$$

which assures the continuity of $E_r \to 0$ on the axis, $r = 0$. Notice that equation (B8) is only a first-step approximation in the computation process and therefore is not identical with the final computed values.

Integration of E_z along the axis gives $V(z)$ and $\dot{z}(z)$. Integration of $\int_{r=0}^{r} E(z = \text{constant}, r\, dr)$ gives $V(r, z = \text{constant})$ with the initial value $V(0, z = \text{constant})$ used as the constants of integration. Mapping of the complete potential field $V(r, z)$ determines the ion velocity $u^2(r, z) = u_o^2 + \dot{z}^2\left[1 + (r')^2\right] + r^2\dot{\theta}_i^2$ from equation (19), with r' yet to be determined. This value of r' can be estimated with the help of equation (B4b). Since the radius of the trajectories is between 0 and about 0.1 meter, the order of magnitude of $r^2\dot{\theta}_e$ is 10 square meters per second. According to equation (14a), $r^2\theta_e$ is equal to e/m times the flux difference $\psi - \psi_o$. Again, for $B \approx 0.3$ tesla and $r < 0.1$ meter, $\frac{e}{m}\psi_o \approx 10^5$ and $\frac{e}{m}\psi \approx r^2\dot{\theta} + \frac{e}{m}\psi_o \approx 10^5 + 10 \approx 10^5$ is obtained. Thus, the substitute electron must follow a trajectory that is close to a tube of constant flux. The latter is easily computed as long as the induced magnetic field is small compared

with that externally applied, and an initial approximation of r' is that which results from constant flux trajectories.

APPENDIX C

DISCUSSION OF BASIC ASSUMPTIONS

In this section, the validity of some basic assumptions made in this study will be checked.

The first assumption concerns the adiabatic conservation of μ. That ΔB incurred during one cyclotron orbit is much smaller than the local value of B will be proved at a position where B is small and thus at the least favorable condition. Select B = 500 gauss; then from B field mapping is found

$$\frac{\partial B}{\partial z} = 50 \text{ G/cm}$$

$$\Delta B = \frac{\partial B}{\partial z} \times \Delta z = \frac{\partial B}{\partial z} u \times \tau_c = 50 \times 4.5 \times 10^6 \times \frac{2}{3} \times 10^{-9} = 0.15 \text{ G},$$

if stream velocity u is approximately 4.5×10^6 centimeters per second and

$$\omega_c = \frac{e}{m} B \approx 9 \times 10^9 \text{ sec}^{-1}$$

and

$$\tau_c = \frac{2\pi}{\omega_c} \approx \frac{2}{3} \times 10^{-9}$$

Therefore,

$$\frac{\Delta B}{B} = \frac{1.50 \times 10^{-1}}{500} = 0.3 \times 10^{-3}$$

which is negligibly small. Thus, μ is conserved down to even much smaller values of B, at which the acceleration process is completed.

Next, it will be proved that the power radiated in cyclotron radiation is small for the conditions assumed here. The cyclotron radiated power is (ref. 8)

$$P_r = \frac{2}{3} \frac{e^4 Z^4 B^2 v_1^2}{4\pi\epsilon_0 c^3 m^2} = \frac{1}{3} \frac{e^4 \times B^3}{\pi\epsilon_0 c^3 m^3} \times \mu \qquad \text{(C1)}$$

because $v_\perp^2 = \frac{2\mu B}{m}$ and $Z = 1$ where Z is the charge number; for $\mu \approx 8\times10^{-12}$ ampere-square centimeter and $B = 3000$ gauss, P_r is 6×10^{-18} watt per electron. With $\dot{N} = 3.65\times10^{18}$ atoms per second, the energy input per particle is 1000 watts per $3.65\times10^{18} \approx 3\times10^{-16}$ joules. The acceleration time is approximately

$$\frac{50 \text{ cm}}{\frac{u}{2}_{max}} \approx \frac{50 \text{ cm}}{2.5\times10^{6} \text{ cm/sec}} \approx 20\times10^{-6} \text{ sec}$$

Even if the electrons radiated at maximum power (they do not because B decays), the radiated energy would be less than $6\times10^{-18}\times20\times10^{-6} = 1.2\times10^{-22}$ joules $<< 3\times10^{-16}$ joules. Equation (C1) is valid for $v_\perp << c$, which is correct for the range of parameters selected for this computation.

REFERENCES

1. Miller, David B.; Bethke, George W.; and Crimi, Giles F.: Investigation of Plasma Accelerator (Cyclotron Resonance Propulsion System). Rep. No. GE 214-252 (Final) (NASA CR-54756), General Electric Co., Nov. 1, 1965.

2. Alfvén, Hannes: Cosmical Electrodynamics. Clarendon Press, Oxford, 1950.

3. Alfvén, Hannes: On the Origin of Cosmic Radiation. Tellus, vol. 6, no. 3, Aug. 1954, pp. 232-253.

4. Hellwig, Gerhard: On the Motion of Charged Particles in Weakly Varying Magnetic Fields. Z. Naturforschung, vol. 10a, 1955, pp. 508-516. (In German.)

5. Kilpatrick, W. D.; Mullins, J. H.; and Teem, J. M.: Propulsion Application of the Modified Penning Arc Plasma Ejector. AIAA J., vol. 1, no. 4, Apr. 1963, pp. 806-813.

6. Pierce, John R.: Theory and Design of Electron Beams. D. Van Nostrand Co., Inc., 1949.

7. Smythe, William R.: Static and Dynamic Electricity. Second ed., McGraw-Hill Book Co., Inc., 1950, p. 267.

8. Sommerfeld, Arnold J. W. (E. G. Ramberg, trans.): Electrodynamics. Vol. 3 of Lectures on Theoretical Physics, Academic Press, 1964, p. 297.

NASA-Langley, 1967 E-3387

"The aeronautical and space activities of the United States shall be conducted so as to contribute . . . to the expansion of human knowledge of phenomena in the atmosphere and space. The Administration shall provide for the widest practicable and appropriate dissemination of information concerning its activities and the results thereof."

—NATIONAL AERONAUTICS AND SPACE ACT OF 1958

NASA SCIENTIFIC AND TECHNICAL PUBLICATIONS

TECHNICAL REPORTS: Scientific and technical information considered important, complete, and a lasting contribution to existing knowledge.

TECHNICAL NOTES: Information less broad in scope but nevertheless of importance as a contribution to existing knowledge.

TECHNICAL MEMORANDUMS: Information receiving limited distribution because of preliminary data, security classification, or other reasons.

CONTRACTOR REPORTS: Technical information generated in connection with a NASA contract or grant and released under NASA auspices.

TECHNICAL TRANSLATIONS: Information published in a foreign language considered to merit NASA distribution in English.

TECHNICAL REPRINTS: Information derived from NASA activities and initially published in the form of journal articles.

SPECIAL PUBLICATIONS: Information derived from or of value to NASA activities but not necessarily reporting the results of individual NASA-programmed scientific efforts. Publications include conference proceedings, monographs, data compilations, handbooks, sourcebooks, and special bibliographies.

Details on the availability of these publications may be obtained from:

SCIENTIFIC AND TECHNICAL INFORMATION DIVISION

NATIONAL AERONAUTICS AND SPACE ADMINISTRATION

Washington, D.C. 20546